Breakdown of shape memory effect in bent Cu-Al-Ni nano-pillars: when twin boundaries become stacking faults

L.F.Liu[1], X. Ding[1*], J. Sun[1], and E. K. H. Salje[1,2*]

[1]*State Key Laboratory for Mechanical Behavior of Materials,*
Xi'an Jiaotong University, Xi'an 710049, China
E-mail: dingxd@mail.xjtu.edu.cn

[2]*Department of Earth Sciences,*
University of Cambridge, Cambridge CB2 3EQ, UK
E-mail: ekhard@esc.cam.ac.uk

Keywords: finite size scaling, shape memory effect, size dependence of shape memory, Cu-Al-Ni alloys.

Abstract

Bent Cu-Al-Ni nano-pillars (diameters 90 nm - 750 nm) show the shape memory effect, SME, for diameters d > 300 nm. The SME and the associated twinning are due to a small deformed section of the nano-pillar. Thick nano-pillars (d>300nm) transform to austenite under heating, including the deformed region. Thin nano-pillars (d < 130 nm) do not twin but generate highly disordered sequences of stacking faults in the deformed region. No SME occurs and heating converts only the un-deformed regions into austenite. The defect-rich, deformed region remains in the martensite phase even after prolonged heating in the stability field of austenite. A complex mixture of twins and stacking faults was found for diameters 130 nm < d < 300 nm. The size effect of the SME in Cu-Al-Ni nano-pillars consists of an approximately linear reduction of the SME between 300nm and 130 nm when the SME completely vanishes for smaller diameters.

All ferroic materials show finite size effects when sample dimensions decrease below some characteristic length and the ferroic effect is destroyed. Such length scales exist in magnetism[1-4] while finite size effects in ferroelectrics are primarily related to the depolarization field[11-14], which tends to destroy the formation of the spontaneous polarization. The typical geometries in ferroelectrics are thin films (critical thickness 10 nm[5, 6]) and thin polymer layers (critical thickness 2.5 nm[7-10]). Finite size effects are also expected in ferroelastic (martensitic) materials and nano-scale shape memory alloys (SMA)[15-20]. Here the ideal geometry for investigations is nano-pillars[21-24] to identify the minimum diameter below which the shape memory effect (SME) is destroyed. Structural arguments lead to such an expectation because the induced nanostructures will change with size: bending of nano-pillars will always lead to the formation of suitable adaptive nanostructures[25] but only some nanostructures, namely twins, contribute to the SME while others do not. If strain induced twinning disappears below a certain length scale, no SME can exist at smaller lengths. Furthermore, complex nano-structures may impede the phase transformation to the austenite phase under heating and thereby also destroy the SME.

We report in this paper experimental results, which show that finite size effects in sheared nano-columns stem indeed from a crossover between twinning in thicker nano-pillars to sequences of disordered stacking faults in thinner ones. This result has considerable technological relevance for the application of super elastic and shape memory effects[19, 20] and the use of SMAs in nano-scale device applications[26, 27]. Furthermore, it shows a size-limit for the generation of twin wall related functionalities such as polar twin walls [25] because the template for polarity, namely the twin wall itself, becomes unstable below a critical thickness of the nano-pillar. This prevents us from the development of high-density ferroelectric memory devices based on twinned nano-pillars with polar twin boundaries[28]. Previous investigations on submicron SMAs[29-31] with diameters 200 nm – 300 nm failed to identify the breakdown of the SME. Here we show that the critical diameter for the breakdown of the SME is indeed smaller than 200nm.

Investigations of size dependent mechanical twinning under compression have already revealed some grain-size dependence[32-42]. The grain size effect of twinning has been reported in nano-crystalline Ni and Cu[33, 38], and has been attributed to the competition between the grain size-dependence of partial dislocations and the layer-by-layer promotion of partial slip near the

surface. Hexagonal close-packed Ti-5%Al (at. %) crystal pillars show that the stress required for deformation twinning increases drastically for compression and samples sizes (~1 μm), below which twins are suppressed and replaced by dislocations[36]. Mechanical twinning in these experiments was driven by compression and studied in structural (non SMA) materials. Our approach is different: firstly we use bending deformations because most SME applications make use of bending rather than compression[43-45]. Secondly, mechanical twinning in conventional materials is different from transformation twinning in SMAs where the twin angles and twin wall energies tend to be much lower than in mechanical twinning. Hence we cannot necessarily extrapolate the results from structural materials to SMAs and the size dependence of the SME is expected to be rather different from that of mechanical twinning experiments.

We employ a JEOL 2100F FEG transmission electron microscopy (TEM) with Hysitron PicoIndenter 95 (PI 95) system of Hystitron™ to measure the shape recovery of bent nano-SM Cu-13.8Al-4.2Ni. We first fabricate pillars of different sizes using dual-beam focused-ion-beam (FIB) with a 15 kV gallium ion-beam and a 30 kV electron-beam. The current was controlled to be 1.5 pA to minimize the contamination of the sample by gallium. We achieve in-plane bending by off-axis compression of 'cane shaped' samples (Figure 1). The length-to-thickness aspect ratios were about 8 for thicknesses D of the pillars below the cane handle between 270 nm and 750 nm. This same aspect ratio was ca. 11 for thinner samples with D between 70 nm the 250 nm. The width of cross-section of all pillars varied between 0.95 and 1.

The off-axis compression leads indeed to the bending of the nano-pillar as shown in Figure 1. The red and blue arrows are the load axis and the central axis along $[\bar{2}11]$, respectively. The bending angle θ is shown in Figures.1b and 1f. The load direction is along the long axis of the martensitic pillars, the rate is $10^{-3}s^{-1}$.[27] The sample was a single crystal Cu-13.8Al-4.2Ni (wt. %). The transformation temperatures from the austenite phase (β_1) to martensite are M_s =318.02 K, M_f=297.98 K, A_s=303.19 K and A_f=328.86 K [16], twin planes are $\{121\}_{\gamma_1'}$

Figure1 shows that bent thick and thin nano-pillars behave fundamentally differently. Full shape recovery under heating occurs for the thick samples (e.g. Figures 1a-d) while samples with thicknesses below 130 nm (Figures 1e-h) show no shape recovery and hence no SME. Selected

area diffraction patterns (SADPs) were undertaken to explore the difference between the straight and bent areas of the thin nano-pillar (Figures 1,2). The SADP of the straight parts of the nano-pillars at room temperature always show the martensitic 2H structure (Figure 2a of a 90nm nano-pillar). The transformation from the martensite phase to austenite is almost complete when the sample is heated to 423K (Figure2b, disappearance of the 2H reflections with [120] zone axis and the appearance of DO_3 reflections with [120] zone axis). A complete transformation to austenite DO_3 is seen after heating to 573 K (Figure 2c). The same transformation behaviour was found for all thick nano-pillars for the straight and the bent regions.

This behaviour is very different for the bent regions of thin nano-pillars (diameter 90 nm in Figure 2d). The SADP at room temperature shows the martensitic 2H structure. The SADP still shows the 2H structure after heating to 423 K. Subsequent heating for 1.5 hours to 573 K only produced minor transformations into the austenite phase but no shape recovery (Figure 2f). The inset in Figure 2f shows the diffraction pattern with a high degree of martensitic deformation just after heating to 573 K. This observation proves that the bent region in this sample contains a large number of non-recoverable defects, which prevent the transformation from martensite to austenite.

The difference between the straight and bent regions in the thin nano-pillars demonstrates that we are indeed investigating the size effect of the SME but not the size effect of the phase transformation between martensite and austenite. This latter size effect would be well below the thickness of our thinnest nano-pillars (90nm) because we find that the straight regions of all samples do indeed transform to austenite under heating. Only when complex nano-structures are generated by bending in the bent regions does the phase transformation to austenite, and hence the SME, disappear.

The deformation mechanism for the thin and thick nano-pillars is now analysed by high-resolution transmission electron microscopy (HRTEM). Figures 3a and 3b show that the structure without lattice deformation is 2H in both the thin and thick nano-pillars. However, in the bent region, only twinning occurs in the thick nano-pillar (Figures 3c and 3d). whereas the bent region in the thin nano-pillar (zone II in Figure 1f) contains complex polytypical stackings.

The HRTEM images in Figure 3e shows a multitude of stacking faults and moiré fringes indicating bent atomic planes. Details of stacking faults are shown in Figure 3f for the areas in the green square of Figure 3c. A diffraction image of the same area (insert in Figure 3e) shows streaks and diffuse scattering. This proves that the polytypic stacking sequences are not well defined but include multiple stacking faults and polytypic stackings with different repetition units. The image in Figure 3e also shows that the planes bent and intersect. This indicates that twinning deformation in thicker samples is replaced by highly disordered stackings in thin nano-pillars. They suppress the martensite to austenite transformation and hence the SME (in contrast to twins in thicker nano-pillars)[46].

The breakdown of the SME has hence nothing to do with the length scale of elastic correlations, nor with the length scale of twin boundary interactions with the surface. Instead we find that bending generates twin boundaries for large samples and complex stacking sequences for thin samples. The energy of twin boundaries is typically slightly smaller than that of stacking faults so that it is not surprising that bulk effects will favour twins (including their surface relaxation [47]) while thin samples favour stacking faults and polytypic transformations. This result can be rationalized by our understanding that the twinning minimizes the global strain energy is hence largely independent of the atomic configurations while stackings minimize the local atomic interaction potentials. With decreasing size, surface relaxations reduce the strain energy so that now the local atomic energies become predominant and favour the development of local stackings. It is also well stablished that both twins and stacking faults are common in Cu-Al-Ni [48]. A previous microscopic model explains the inhibition of the martensitic transformation in bulk Cu-Al-Ni, related to the localized interaction between a dislocation array and the twinned γ_1' structure. This model takes into account the interaction between the martensitic stress-free transformation strains and the stress field created by the dislocation arrays [49,54]. Interactions between twin boundaries and stacking faults [51] and changes of stacking sequences during the martensitic transformation in Cu-Zn-Al SMAs are reported in [52] and the coexistence of twins and stacking faults in [53].

In summary, the finite size scaling of the SME is a consequence of the mixture of these two features: twinning is reversible under heating to the austenite phase but disordered stacking faults

are not and even prevent the phase transformation altogether. In the intermediate regime, stacking faults may prevent twins from moving [54] and partially stabilize the 2H structure. The experimentally determined size dependence of the SME is shown in Figure 4. No size dependence was found for samples with diameters larger than 300 nm when the SME is generated by twinning. An approximately linear decay was found between 350nm and 130nm when the SME is reduced from 90 % to zero. No SME was found for samples thinner than 130 nm with complex stacking sequences dominating the bent regions. Applications of SMAs in miniaturized micro- and nano-electromechanical systems (MEMS/NEMS) are hence limited to samples bigger than the cut-off length (here 130nm). Twin wall related functionalities are also impossible to observe in the thinnest nano-pillars simply because twin walls seize to exist in the thinnest samples.

Acknowledgment

This work was supported by the National Natural Science Foundation of China (Grant Nos. 51171140, 51231008, 51321003and 51320105014), the 973 Program of China (2012CB619402), the 111 Project of China (B06025), and EPSRC (EP/K009702/1). The authors thank Xiaolei Wu for helpful discussion on this paper.

References

(1) Kubota, T.; Mizukami, S.; Watanabe, D.; Wu, F.; Zhang, X.; Naganuma, H.; Oogane, M.; Ando, Y.; Miyazaki, T.; J. Phys. D 2013, **46**,155001.

(2) Ślęzak, M.; Ślęzak, T.; Freindl, K.; Karaś, W.; Spiridis, N.; Zając, M.; Chumakov, A. I.; Stankov, S.; Rüffer, R.; Korecki, J.; Phys. Rev. B 2013, **87**, 134411.

(3) Papaioannou, E. Th.; Kapaklis, V.; Taroni, A.; Marcellini, M.; Hjörvarsson, B.; J. Phys. Cond. Matter. 2010, **22**, 236004.

(4) R. F. Barrow, Contemp. Phys. Taylor & Francis LTD, 1984, **25**, pp.200-201.

(5) Karasawa, J.; Sugiura, M.; Wada, M.; Hafid, M.; Fukami, T.; Integr. Ferroelectr. 1996, **12**, 105-114.

(6) Ducharme, S.; Fridkin, V. M.; Bune, A.V.; Palto, S. P.; Blinov. L. M.; Petukhova, N. N.; Yudin, S. G.; Phys. Rev. Lett. 2000, **84**, 175-178.

(7) Choi, J.W.; Dowben, P.A.; Pebley, S.; Bune, A. V.; Ducharme, S.; Fridkin, V. M.; Palto, S. P.; Petukhova, N.; Phys. Rev. Lett. 1998, **80**, 1328-1331.

(8) Vizdrik, G.; Ducharme, S.; Fridkin, V.M.; Yudin, S. G.; Phys. Rev. B 2003,**67**, 094113.

(9) Ducharme, S.; Reece, T. J.; Othon, C.M.; Rannow, R. K.; IEEE Transactions devices and materials reliability 2005, **5**, 720-735.

(10) Reece, T.J.; Ducharme, S.; Sorokin, A.V.; Poulsen, M.; Appl. Phys. Lett. 2003, **82**, 142-144

(11) Scott, J.F.; Dearaujo, C.A.P.; Science 1989, **246**, 1400-1405.

(12) Scott, J. F.; Duiker, H.M.; Beale, P.D.; Pouligny, B.; Dimmler, K.; Parris, M.; Butler, D.; Eaton, S.; Physica B & C 1988, **150**, 160-167.

(13) Zhong, W.L.; Wang, Y.G.; Zhang, P.L.; Qu, B.D.; Phys. Rev. B 1994, **50**, 698-703.

(14) Zhao, Z.; Buscaglia, V.; Viviani, M.; Buscaglia, M. T.; Mitoseriu, L.; Testino, A.; Nygren, M.; Johnsson, M.; Nanni, P.; Phys. Rev. B 2004, **70**, 024107.

(15) Otsuka, K.; Wayman, C.M.; Cambridge University Press (New York) 1999**,** pp. 27–33.

(16) Huang, W.; Ding, Z.; Wang, C.; Wei, J.; Zhao, Y.; Purnawali, H.; Mater. Today 2010**, 13**, 54.

(17) Otsuka, K.; Ren, X.; Prog. Mater. Sci. 2005**, 50**, 511-678.

(18) Ng, K.; Sun, Q.; Mech. Mater. 2006, **38**, 41-56.

(19) Liu, Y.; Li, Y.; Xie, Z.; Ramesh, K.; Philos. Mag. Lett. 2002, **82**, 511-517.

(20) Salje, E. K. H.; Annu. Rev. Mater. Res. 2012**, 42**, 265-283.

(21) Maass, R.; Wraith, M.; Uhl, J.T.; Greer, J.R.; Dahmen, K. A.;Phys. Rev. E 2015, **91,** 042403.

(22) Wendy Gu, X.; Loynachan, C. N.; Wu, Z.; Zhang, Y.; Srolovitz, D. J.; Greer, J. R.; *Nano Letters* 2012, **12**, 6385-6392.

(23) Gu, X.W.; Jafary-Zadeh, M.; Chen, D.Z.; Wu, Z.; Zhang, Y.W.; Srolovitz, D.J.; Greer, J.R.; Nano Letters 2014, **14,** 5858–5864.

(24) Jang, D.; Li, X.; Gao, H.; Greer, J.R.; Nat. Nanotechnology 2012, **7**, 594-601.

(25) Viehland, Dwight D.; Salje, E. K. H.; Adv. Phys. 2014, 63, 267-326.

(26) Carpena-Nunez, J.; Yang, D.; Kim, J.; Park, C.; Fonseca, L.; Nanotechnology 2013**, 24**, 035701.

(27) Lu, Y.; Peng, C.; Ganesan, Y.; Huang, J. Y.; Lou, J.; Nanotechnology 2011, **22,** 355702.

(28) E.K.H. Salje, Chemphyschem 2010, **11**, 940-950.

(29) San Juan, J.; No, M. L.; Schuh, C.A.; Adv. Mater. 2008, **20,** 272-278.

(30) Zhong, Y.; Gall, K.; Zhu, T.; Acta Mater. 2012, **60**, 6301.

(31) Clark, B. G.; Gianola, D. S.; Kraft, O.; Frick, C.P.; Adv. Eng. Mater. 2010,**12,** 808-815.

(32) Wu, X.; Zhu, Y.; Phys. Rev. Lett. 2008, **101,** 025503.

(33) Seo, J. H.; Park, H. S.; Yoo, Y.; Seong, T. Y.; Li, J.; Ahn, J. P.; Kim, B.; Choi, I. S.; Nano Lett. 2013, **13,** 5112-5116.

(34) Zhu, Y.; Liao, X,; Wu, X.; Prog. Mater. Sci. 2012, **57,** 1-62.

(35 Yu, Q.; Shan, Z. W.; Li, J.; Huang, X.; Xiao, L.; Sun, J.; Ma, E.; Nature 2010, **463**, 335-338.

(36) Yu, Q.; Qi, L.; Chen, K.; Mishra, R. K.; Li, J.; Minor, A. M.; Nano Lett. 2013, **12,** 887-892.

(37) Zhang, J. Y.; Liu, G.; Wang, R. H.; Li, J.; Sun, J.; Ma, E.; Phys. Rev. B 2010, **81,** 172104.

(38) Zhang, J.; Wei, Y.; Sun, T.; Hartmaier, A.; Yan, Y.; Li, X.; Phys. Rev. B 2012, **85,** 054109.

(39) Zhang, J. Y.; Zhang, P.; Wang, R. H.; Liu, G.; Zhang, G. J.; Sun, J.; Phys. Rev. B 2012, **86,** 064110.

(40) Sedlmayr, A.; Bitzek, E.; Gianola, D. S.; Richter, G.; Monig, R.; Kraft, O.; Acta Mater. 2012, **60,** 3985-3993.

(41) Christian, J. W.; Mahajan, S.; Prog. Mater. Sci. 1995, **39,** 1-157.

(42) Minor, A. M.; Asif, S. A. S.; Shan, Z.; Stach, E. A.; Cyrankowski, E.; Wyrobek, T. J.; Warren, O.; Nat. Mater. 2006**, 5,** 697-702.

(43) Carpena-Núñez, J.; Yang, D.; Kim, J. W.; Park, C.; Fonseca, L. F.; Nanotechnology, 2013, **24**, 035701.

(44) Lu, Y.; Peng, C.; Ganesan, Y.; Huang, J.Y.; Lou, J.; Nanotechnology, 2011, **22**, 355702.

(45) Lu, Y. H.; Liang, S.; Chu, W.Y.; Qiao, L.J.; Intermetallics, 2002, **10**, 823-827.

(46) Salje, E.; Palosz, B.; Wruck, B.; J. Phys. C 1987, **20**, 4077-4096.

(47) Novak, J.; Salje, E.K.H.; J. Phys. Condens. Matter 1998, **21**, L359-L366.

[48] Zhang, G. F.; Sauvage, X.; Wang, J. T.; Gao, N.; Langdon, T. G.; J. Mater. Sci. 2013, **48**, 4613-4619.

(49) Gastien, R.; Sade, M.; Lovey, F. C.; Shape Memory Alloys: Manufacture, Properties and Applications, 2010, pp:145-180 .

(50) Gastien, R.; Sade, M.; Lovey, F.C.; Mater. Sci. Eng. A 2008, **481**, 518-521.

(51) Condo, A. M.; Lovey, F. C.; Torra, V.; Phil. Mag. 2003, **83**, 1479-1493

(52) Stoiber, J.; Gotthard, R.; Mater. Sci. Eng. A 1993, **164**, 443-448 .

(53) Wang, R.; Luo, C.; Gui, J.; Ren, Q.; Chen, J.; J. Phys. Condens. Matter 1992, **4**, 2397-2403.

(54) Salje, E. K. H.; Zhang, H.; Idrissi, H.; Schryvers, D.; Carpenter, M. A.; Moya, X.; Planes, A.; Phys. Rev. B 2009, **80**, 134114 .

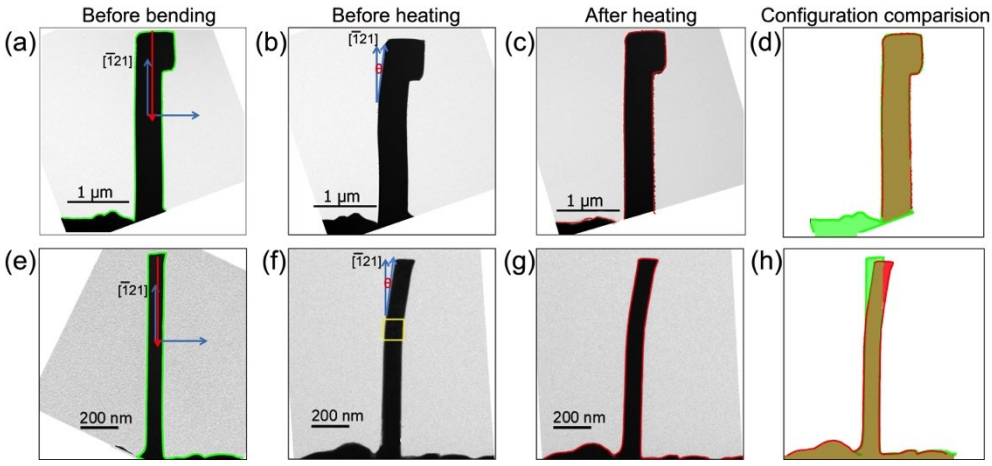

Figure 1 Shape memory behavior of nano-pillars of Cu-13.8Al-4.2Ni with a bending axis [$\bar{2}$ 11], the bending angle is θ_1=8.0° and for large and θ_2=7.5° for thin pillars. a-d: shape recovery of a large pillar with lateral cross-section width D = 470 nm, height 3326 nm (including the cane shape part). e-h: shapes of a thin pillar with D = 90 nm, height 1005 nm with no shape recovery after heating.

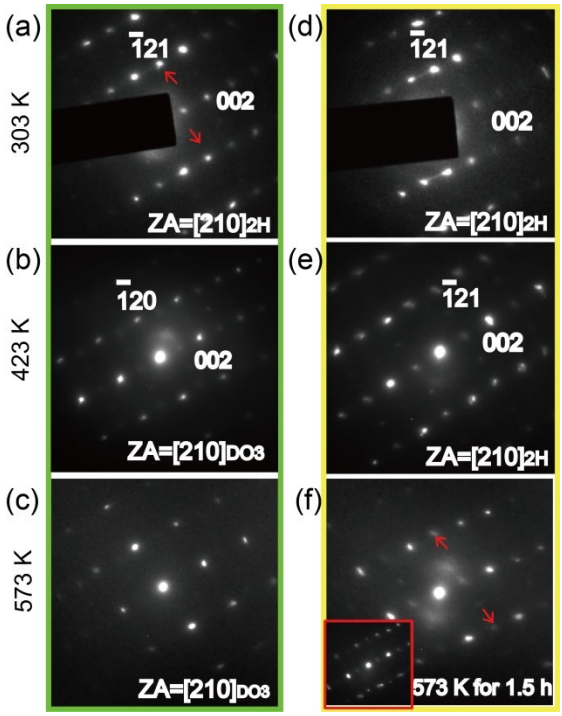

Figure 2 Diffraction patterns of straight (a, b, c) and bent (d, e, f) regions of a thin pillar during heating (thickness 90nm). SADP of the martensite 2H structure in the straight region at 303K (a) and at 423K (b). The with complete transformation from martensite to austenite is seen by the disappearance of 2H reflections and the appearance of DO_3 reflections (b), complete recovery at 573 K (c). SADP of the bent region at 303K (d) also shows that the 2H structure does not change after heating to 423K(e). Some incomplete transformation is seen after heating to 573K for 1.5 hours (f). The inset in f shows the diffraction pattern directly after heating to 573K with no recovery.

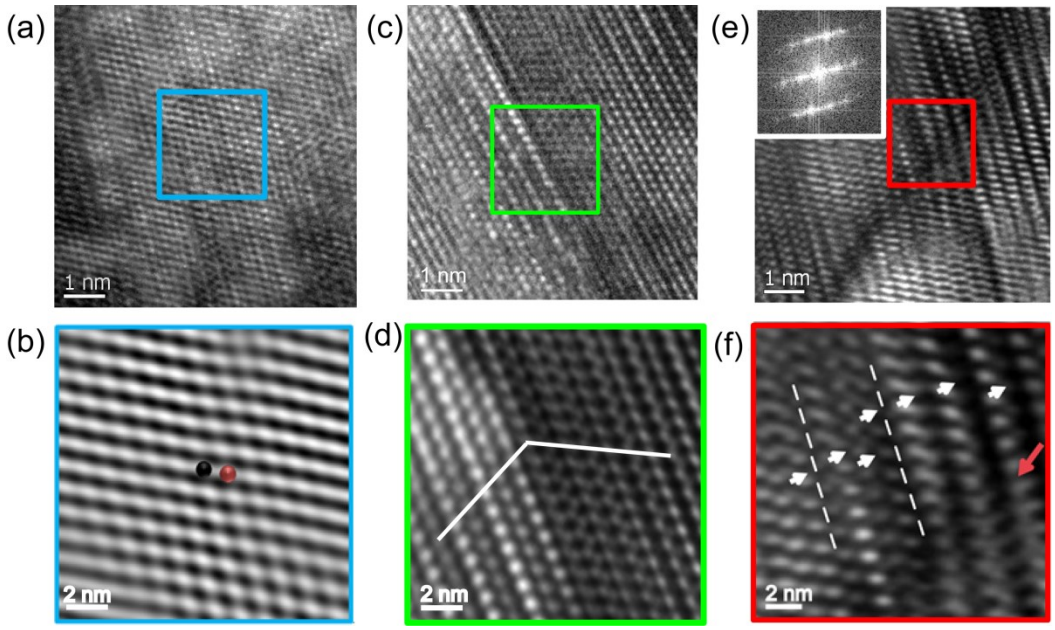

Figure 3 HRTEM of underformed pillars (a,b) and the bent region of a thick (c,d), and a thin pillar (e,f). (a) The structure of underformed pillars and inverse fast Fourier transformation (IFFT) of the area in the blue frame (b) show the ABAB stacking of the martensite 2H phase. Twins appear in the bent region of a thick pillar (c) and the IFFT (d) Twinned lattice planes are shown by white lines. Multiple stacking faults (white arrows and highlighted by the dash line) dominate the bent region in thin pillars (e,f). The diffraction pattern (insert) of the full region shows highly diffuse scattering due to high concentrations of lattice imperfections.

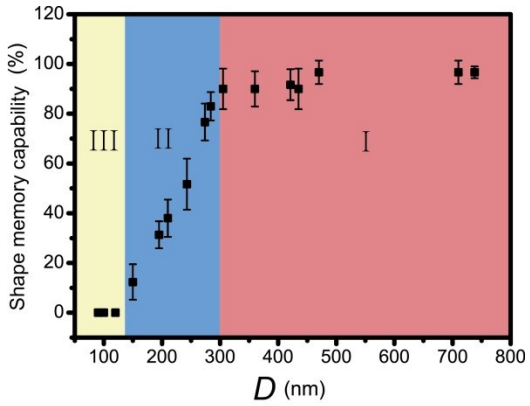

Figure 4 Finite size scaling of the degree of shape recovery in bent CuAlNi nano pillars. No shape recovery occurs below 130 nm while full recovery occurs for sizes larger than 300 nm. In the intermediate crossover regime we find a linear increase of the shape recovery with increasing size (recoverability is defined by $(\theta-\theta')/\theta'$ where $(\theta-\theta')/\theta'$ and θ' are the bending angles before and after heating (see Figure1).